

Hyperspectral quantification of wheat resistance to *Fusarium* head blight: comparison of two *Fusarium* species

E. Alisaac · J. Behmann · M. T. Kuska · H.-W. Dehne ·
A.-K. Mahlein

Accepted: 3 May 2018 / Published online: 19 May 2018
© Koninklijke Nederlandse Planteziektenkundige Vereniging 2018

Abstract Interactions of *Fusarium* species with different wheat varieties differ in their temporal dynamics and symptom appearance. Reliable and objective approaches for monitoring processes during infection are demanded for plant phenotyping and disease rating. This study presents an automated method to phenotype wheat varieties to *Fusarium* head blight (FHB) using hyperspectral sensors. In time-series experiments, the optical properties of spikes infected with *F. graminearum* or *F. culmorum* were recorded. Two hyperspectral cameras, in visible and near-infrared (VIS-NIR, 400–1000 nm) and shortwave-infrared (SWIR, 1000–2500 nm) captured the most relevant bands for pigments, cell structure, water and further compounds. Correlations between disease severity (DS), spike weight, spectral bands and vegetation indices were investigated. Following, the detectability of infections was assessed by Support Vector Machine (SVM) classifier. A variety ranking based on AUDPC

was performed and compared to a fully-automated approach using Non-metric Multi-Dimensional Scaling (NMDS). High correlation was found between the spectral signature and DS in 430–525 nm, 560–710 nm and 1115–2500 nm. All indices from the VIS-NIR showed high correlation with DS and, for the first time, this was also confirmed for three indices from the SWIR: NDNI, CAI and MSI. Using SVM, differentiation between healthy and infected spikes was possible (acc. > 0.76). Furthermore, the possibility to differentiate between *F. graminearum* and *F. culmorum* infected spikes has been verified. The NMDS approach was able to reproduce accurately the variety ranking and outlines the potential of hyperspectral imaging to phenotype the variety susceptibility for improved breeding processes.

Keywords Wheat · *F. graminearum* · *F. culmorum* · Phenotyping · Hyperspectral imaging · Spectral signature · Spectral vegetation indices (SVIs) · Support vector machine (SVM) · AUDPC · Non-metric multidimensional scaling (NMDS)

Electronic supplementary material The online version of this article (<https://doi.org/10.1007/s10658-018-1505-9>) contains supplementary material, which is available to authorized users.

E. Alisaac · J. Behmann (✉) · M. T. Kuska ·
H.-W. Dehne · A.-K. Mahlein
Institute of Crop Science and Resource Conservation (INRES),
Plant Diseases and Plant Protection, Rheinische
Friedrich-Wilhelms Universität Bonn, Nussallee 9, 53115 Bonn,
Germany
e-mail: jbehmann@uni-bonn.de

A.-K. Mahlein
Institute of Sugar Beet Research (IfZ), Holtenser Landstraße 77,
37079 Göttingen, Germany

Introduction

Fusarium head blight (FHB) is considered as one of the most important fungal diseases of wheat, because it causes high crop losses and can lead to high economic losses (Johnson et al. 2003; McMullen et al. 2012; Salgado et al. 2015). In addition, kernels of infected spikes are small, shrunken, discolored and light in weight and the technological quality is also affected

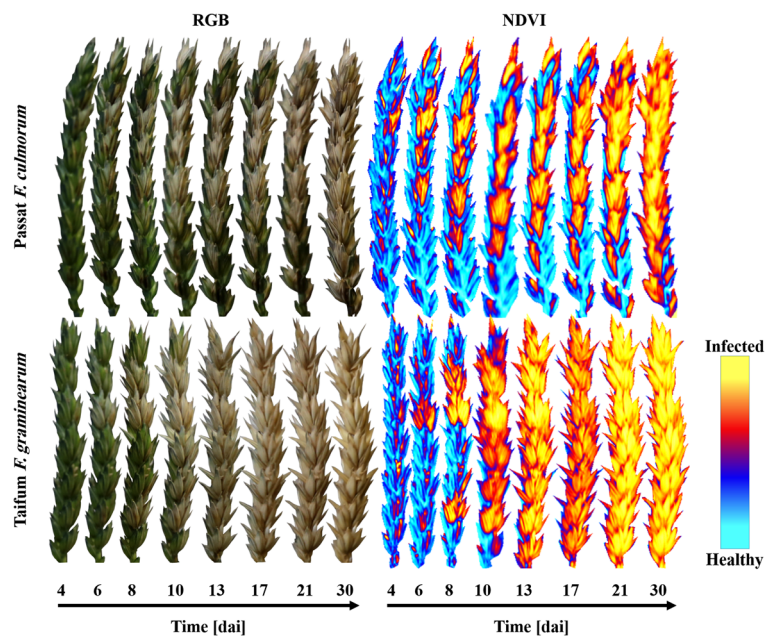
(McMullen et al. 2012; Kreuzberger et al. 2015). The most important *Fusarium* species inducing FHB are *Fusarium graminearum*, *F. culmorum*, *F. poae*, *F. avenaceum*, *F. sporotrichoides*, *F. equiseti* (Parry et al. 1995; O'Donnell et al. 2004; Aoki et al. 2014).

In wheat, FHB infection is initiated by airborne spores resulting from the mycelium and from debris of the former crop. Infection may take place during flowering, preferably at warm temperature $>25\text{ }^{\circ}\text{C}$ with 100% relative humidity (RH). The germ tubes of conidia enter the spikelet tissue through the natural openings in the spikelet and the degrading anther tissue (Bushnell et al. 2003; Osborne and Stein 2007). First symptoms appear on infected spikelets as water-soaked spots. With ongoing disease development, the chlorophyll decomposes and the whole spikelet becomes bleached. In warm humid weather, pinkish-red mycelium and conidia develop in the infected spikelets (Trail 2009). The infection spreads to adjacent spikelets horizontally and vertically, up and down through the entire spike (Fig. 1) (Ribichich et al. 2000; Brown et al. 2010; Al Masri et al. 2017). The main reason to focus on FHB is its ability to produce mycotoxins. Mycotoxins secreted by *Fusarium* species are toxic and detrimental to humans and animal nutrition (McCormick 2003; Pestka 2010). The main mycotoxins produced by these species are trichothecenes, mainly deoxynivalenol (DON) and its

derivatives as well as zearalenone, fusaric acid, fusarenon or enniatins (Birzele et al. 2002; Ferrigo et al. 2016).

In order to achieve an effective management of FHB, different control strategies must be combined. Integrated crop protection strategies include cultural practices such as crop rotation, biological control or fungicides application (Gilbert and Haber 2013). Thereby, breeding of resistant wheat varieties contributes to the integrated control of FHB (Dweba et al. 2017). These varieties should combine both types of FHB resistance (Mesterházy et al. 2007), i.e. Type I resistance (resistance to initial infection (penetration)), and Type II resistance (resistance against pathogen spread from the point of infection) (Schroeder and Christensen 1963). Effective resistance breeding needs interdisciplinary research, integrating plant breeding, phytopathology, informatics and long investigation time. To achieve resistant varieties, an important step in breeding programs after generating a new genetic variation is phenotyping. This approach relies on precise visual assessment of the disease severity after artificial inoculation (Steiner et al. 2017). According to Furbank and Tester (2011), precise and innovative methods for identifying and characterising disease symptoms in an early stage of infection are needed. Until today, the phenotyping process is still a limiting factor in plant breeding, because it is time-consuming,

Fig. 1 Visual symptoms of FHB on moderately resistant variety (Passat) and susceptible variety (Taifun) in different development stages of the disease, with NDVI visualization



and cost intensive (Mahlein 2016). In case of FHB, this process is especially challenging as *Fusarium* species can infest the wheat spike and produce mycotoxins without developing visual symptoms. Within this context, optical sensors beyond the capability of the human eye are beneficial to improve phenotyping (Kuska and Mahlein 2018).

Various sensors are applied for the detection, identification and quantification of plant diseases like thermography, fluorescence and hyperspectral sensors (Mahlein 2016). Recently hyperspectral imaging has shown to be useful as a precise and non-destructive tool in characterising resistance to powdery mildew in barley, and in lesion characterization in *Cercospora beticola*–sugar beet interaction (Leucker et al. 2016; Thomas et al. 2016; Kuska et al. 2017). One of the challenges in hyperspectral imaging is the high dimensionality and massive amount of data (Behmann et al. 2015; Fahlgren et al. 2015; Thomas et al. 2018). Spectral vegetation indices (SVIs) are a straightforward approach to reduce the data dimensionality relying on only few specific wavelengths. Qualitative and quantitative information concerning the plant pigments, biomass, tissue structure, water content and plant chemicals can be obtained using these indices (Xue and Su 2017). SVIs showed a good capability to detect FHB on wheat and to discriminate sugar beet diseases caused by *Cercospora* leaf spot, powdery mildew and leaf rust (Bauriegel et al. 2011; Mahlein et al. 2012). Moreover, they have been used as features in support vector machine (SVM) approach to classify sugar beet leaves infected with different pathogens (Rumpf et al. 2010).

The hypothesis of this study is, that wheat varieties differ in their susceptibility to FHB, and that these differences can be determined and assessed by hyperspectral imaging. Therefore, hyperspectral images of different wheat varieties inoculated with *F. graminearum* or *F. culmorum* were taken in the spectral range from 400 to 2500 nm during the pathogenesis. A set of fifteen SVIs were used in SVM classification to discriminate healthy, *F. graminearum* and *F. culmorum* infected spikes. Furthermore, a selection of SVIs was used in non-metric multidimensional scaling (NMDS) to rank wheat varieties according to their susceptibility to FHB.

This study is designed to improve non-destructive and non-invasive screening methods for FHB resistance using the application of hyperspectral imaging technique.

Material and methods

Plant cultivation

Greenhouse experiments were performed using seven varieties of spring wheat (*Triticum aestivum* L.) with different resistant degrees to FHB (ranging from 1 to 9 scale where 1 is highly resistant and 9 is highly susceptible): Thasos (3) (Strube, Söllingen, Germany), Triso (4) (DSV, Lippstadt, Germany), Passat (4), Scirocco (4), Chamsin (5), Taifun (6) (KWS, Einbeck, Germany) and Sonett (6) (Syngenta, Basel Switzerland) (Descriptive List of Varieties, Bundessortenamt, Germany 2017). Pots of 12 × 12 × 20 cm size were filled with a mixed substrate 1:3:6 of sand, horizon C and potting substrate ED 73 (Einheitserde, Sinntal-Altengronau, Germany). Five seeds per pot were cultivated at 20 ± 2 °C and 50–70% RH (two pots for each variety). Pots were randomized in the green house and supplemental artificial light (>300 μmol m⁻² s⁻¹, Philips SGR 140, Hamburg, Germany) was used to obtain a photoperiod of 16/8 h (day/night). After germination, two seedlings were left per pot and were supported by sticks to avoid lodging. Plants were watered as necessary.

Fusarium inoculation and disease severity assessment

Fusarium graminearum, isolate S.19, and *F. culmorum*, isolate 3.37 were used for inoculation (INRES-Plant Diseases and Plant Protection, University of Bonn, Germany). The isolates were obtained from infected wheat kernels from field experiments (Campus Klein-Altendorf, Rheinbach, Germany) in 2011 and 2004, respectively. They were stored as a cryo-culture at –80 °C. Inoculum was produced according to the method of Moradi (2008) using potato dextrose agar (PDA, 39 g L⁻¹), potato dextrose broth (PDB, 24 g L⁻¹) and low strength potato dextrose agar (LSPDA, 12.5 g L⁻¹ and agar-agar 19.5 g L⁻¹). Conidia were harvested in water and the inoculum suspensions were adjusted to 10⁵ conidia mL⁻¹ using a Fuchs–Rosenthal chamber.

Spikes of four plants of each variety were inoculated at plant growth stage (GS) 61–65 according to Lancashire et al. (1991), with each *Fusarium* species separately by spraying the inoculum suspension until run off. In addition, four control plants of each variety were mock inoculated with water. For optimal infection, plants were incubated at 22–25 °C and 95% RH for 48 h, by covering each treatment by a plastic bag according to

Mesterházy et al. (2015). After incubation, six spikes of each treatment were fixed on a black metal grid in order to keep the spikes in the same orientation along the time of the experiment. Spikes were sprayed with tap water until runoff every day, which kept the spikes wet for 1–2 h per day to provide appropriate conditions for disease development.

The disease severity (DS) was assessed according to the formula of Stack and McMullen (1995) 4, 6, 8, 10, 13, 17, 21 and 30 days after-inoculation (dai).

disease severity

$$= \frac{\text{symptomatic area of the spike}}{\text{whole area of the spike}} * 100 \quad (1)$$

Reduction in spike weight was calculated as following:

spike weight reduction

$$= \frac{\text{spike weight}_{\text{control}} - \text{spike weight}_{\text{infected}}}{\text{spike weight}_{\text{control}}} * 100 \quad (2)$$

Correlations and statistically significant differences between treatments in spike weight were calculated using RStudio. Spike Weight data were analysed by standard analysis of variance (ANOVA) with a significance level $p \leq 0.05$, $n = 6$.

Hyperspectral imaging

Hyperspectral imaging was performed with artificial illumination at 4, 6, 8, 10, 13, 17, 21 and 30 (dai). The reflectance of the spikes was recorded in the spectral range from 400 to 1000 nm using the hyperspectral camera ImSpector V10E (Spectral Imaging Ltd., Oulu, Finland) with a spectral resolution up to 2.8 nm and a sensor pixel size of 0.0074 mm which results in a spatial resolution of 0.219 mm per pixel. A spectral binning of 4 was used resulting in 211 hyperspectral bands. A SWIR-Camera (ImSpector N25E, Spectral Imaging Ltd., Oulu, Finland) with a spectral resolution up to 5.8 nm resulting in 256 hyperspectral bands was used to record hyperspectral images in the spectral range from 1000 to 2500 nm. The spatial resolution is 1.02 mm per pixel with 320 pixels per scan line. Both cameras and the illumination system were mounted on a motorized line scanner (Velmex BiSlide, Velmex Inc., Bloomfield, USA). Camera settings and the control of the motorized line scanner were adapted using the SpectralCube software (Spectral

Imaging Ltd., Oulu, Finland). For hyperspectral imaging, spikes were laid horizontally with a homogeneous background. A homogeneous illumination was realized with six ASD-Pro-Lamps (Analytical Spectral Devices Inc., Boulder, Colorado, USA) in a distance of 665 mm and a 45° vertical slope to the spikes.

The whole setup was preheated for 30 min before image acquisition in order to get constant and reproducible illumination conditions. The cameras were focused manually and the exposure time was adjusted to the object. For image reflectance calculation four images were taken: A white reference bar (Spectral Imaging Ltd., Oulu, Finland) which reflects ~99% of the radiated light. Subsequently, a dark current image was recorded by closing an internal shutter of the camera. Finally, the image of the spikes was taken with a subsequent second dark current image. The software “Processing Inspector 3.1” (Geoscap, Cologne, Germany) was used to calculate the reflectance from white reference and dark current measurements. The signals from hyperspectral images were smoothed by applying the Savitzky-Golay filter (25 centred supporting points and a third degree polynomial). Masking and visualizing of image data was done using HSVaP (“Hyperspectral Visualization and Processing”), an Open Source software for supervised and unsupervised analysis of hyperspectral images. The program was initially developed in the IGG-Geoinformation, University of Bonn, and its development is continued in the INRES-Plant Diseases and Plant Protection department (available at <http://www.ikg.uni-bonn.de/forschung/hsvap.html>). It combines training data generation by active learning, clustering, classification and feature weighting in a uniform dataflow based on pure Java and established machine learning libraries. Calculation of mean spectral reflectance was done by MATLAB 2013a.

Spectral vegetation indices

In order to investigate the correlation between SVIs and FHB infection, fifteen vegetation indices related to different physiological parameters were calculated from the visible (VIS), the near infrared (NIR) and the short-wave infrared (SWIR) ranges (Table 1). In the following text, the defined abbreviations for the indices are used. The full description can be found within Table 1. Pearson’s correlation coefficient was calculated in RStudio to investigate the relationship between SVIs and DS.

Table 1 Spectral vegetation indices used in this study: Equations, biological indicator and the references are given

Index	Equation	Indicator	Reference
modified Simple Ratio	$mSR = (R_{750} - R_{445}) / (R_{705} + R_{445})$	Green biomass	Sims and Gamon (2002)
Normalized Differences Vegetation Index	$NDVI = (R_{800} - R_{670}) / (R_{800} + R_{670})$	Biomass, leaf area	Rouse et al. (1974)
Photochemical Reflection Index	$PRI = (R_{531} - R_{570}) / (R_{531} + R_{570})$	Epoxidation state of xanthophyll cycle; pigments and photosynthetic radiation use efficiency	Gamon et al. (1992)
Structure Insensitive Pigment Index	$SIPI = (R_{800} - R_{445}) / (R_{800} + R_{680})$	Carotenoid: chlorophyll a ratio	Peñuelas et al. (1995)
Pigment Specific Simple Ratio	$PSSRa = R_{800} / R_{680}$	Chlorophyll a	Blackburn (1998a, b)
	$PSSRb = R_{800} / R_{635}$	Chlorophyll b	
	$PSSRc = R_{800} / R_{470}$	Carotenoids	
Pigment Specific Normalized Difference	$PSNDa = (R_{800} - R_{680}) / (R_{800} + R_{680})$	Chlorophyll a	Blackburn (1998a, b)
	$PSNDb = (R_{800} - R_{635}) / (R_{800} + R_{635})$	Chlorophyll b	
	$PSNDc = (R_{800} - R_{470}) / (R_{800} + R_{470})$	Carotenoids	
Plant Senescence Reflectance Index	$PSRI = (R_{680} - R_{500}) / R_{750}$	Plant senescence	Merzlyak et al. (1999)
Water Index	$WI = R_{900} / R_{970}$	Water content	Peñuelas et al. (1997)
Moisture Stress Index	$MSI = (R_{1599} / R_{819})$	Water stress	Hunt and Rock (1989)
Cellulose Absorption Index	$CAI = 0.5 (R_{2000} + R_{2200}) - R_{2100}$	Cellulose	Nagler et al. (2003) Daughtry (2001)
Normalized Difference Nitrogen Index	$NDNI = [\log(1/R_{1510}) - \log(1/R_{1680})] / [\log(1/R_{1510}) + \log(1/R_{1680})]$	Nitrogen	Serrano et al. (2002)

Support vector machine classification

Two class classification (healthy /infected) and multiclass classification (healthy/ *F. graminearum* /*F. culmorum*) were performed both in RStudio using values of twelve calculated SVIs in VIS-NIR range and alternatively, using the whole spectral reflectance (432 bands). For the identification of FHB diseases, 1/3 of the data was selected randomly as training data to learn Support Vector Machine (SVM) classifier with Radial Basis Function (RBF) kernel (Cortes and Vapnik 1995). A grid-based approach was applied to optimize the parameter cost (C) and gamma (γ) to specify the best radial basis function. The test data was separated from the training data to evaluate the model by a cross-validation. Important performance measures were the overall accuracy of the model and the sensitivity which gives the proportion of the correctly classified spikes of each class.

Multi-dimensional scaling for information compression

A high number of suitable vegetation indices for the detection of plant stress, senescence and bleaching from the VIS, NIR and SWIR spectral reflectance were investigated in this study. Each of these mathematical formulas

provides a slightly different view on parameters of interest from hyperspectral data. To extract an informative description of the plant’s state or plant diseases, a single index is not enough but the comprehensive information of multiple indices needs to be combined (Mahlein et al. 2010; Rumpf et al. 2010; Behmann et al. 2015).

Non-metric multidimensional scaling (NMDS) is an unsupervised method to define a non-parametric transformation between an original space and a target space with defined dimensionality by minimizing the change in the inter-point Euclidean distances d_{ij} , measured by “Stress” (Kruskal 1964).

$$Stress_D(x_1, x_2, \dots, x_N) = \left(\frac{\sum_{i,j} (d_{ij} - \|x_i - x_j\|)^2}{\sum_{i,j} d_{ij}^2} \right)^{1/2} \tag{3}$$

Based on a dissimilarity matrix D , the stress is minimized by a gradient descent approach leading to the transformed data points x in the target space with desired dimensionality (Borg and Groenen 2005). The resulting coordinates are not fixed with respect to rotation or translation as only the distances between the data points are regarded. Here, NMDS was used to compress the

information of the seven most relevant vegetation indices in a one-dimensional ordinal scale representing the disease severity sensed by the hyperspectral camera. The rating of the respective variety control group was subtracted to remove the effect of natural senescence.

Results

Disease severity

In all varieties senescence started in healthy spikes from 21 dai. First FHB symptoms appeared on all inoculated varieties 4 dai (Fig. 1). The disease severity of *F. graminearum* started <20% in all varieties and developed gradually. In Scirocco, severe symptoms have been shown already 4 dai with a disease severity >60% (Fig. 2). The infection increased gradually in moderate resistant varieties until the end of the experiment, whereas the infection increased rapidly in susceptible varieties. The disease severity was >50% in Scirocco, Taifun and Thasos from 8 dai. The disease severity of *F. culmorum* was lower than of *F. graminearum* in all tested varieties except Chamsin. The infection increased rapidly in Chamsin and Taifun and the disease severity was >50% 10 dai. Finally, the high susceptible varieties had completely bleached spikes 13 dai (Fig. 1).

Progress of spectral signature of control and FHB infected spikes

Mean spectral signatures of control spikes in all varieties were similar from 4 to 8 dai (Fig. S1a). Taifun showed a slight increase in VIS and SWIR reflectance from 10 dai (Fig. S1b). The similarity in spectral signature of control spikes lasted until 21 dai (Fig. S1c). Due to differences in senescence state, significant differences in spectral signatures can be shown 30 dai.

Changes in spectral signatures of *F. graminearum* infected spikes appeared from 4 dai (Fig. 3a). The susceptible variety Scirocco showed higher reflectance in the spectral range 460–670 nm and in the SWIR. With ongoing disease development, spectral signatures differed according to the resistance of the varieties starting from 8 dai (Fig. 3b). The highly susceptible varieties Scirocco and Taifun showed an increased reflectance along the whole spectral range. In contrast, a slight increase in reflectance intensity has been shown in the moderate resistant varieties Chamsin and Passat (Fig. 3b).

Varieties infected with *F. culmorum* showed less differences in spectral signatures. The susceptible variety Taifun showed an increased reflectance from 550 to 670 nm and in the SWIR from 4 dai (Fig. 3d). This reflectance pattern became more prominent 13 dai (Fig. 3e). Passat showed an increased reflectance over the whole spectrum during the experimental period (Fig. 3d–f). Whereas, moderate resistant varieties showed later increase of the reflectance in VIS and SWIR and with a different spectral pattern.

All varieties infected with any of *Fusarium* species showed lower reflectance in NIR range comparing to control spikes starting at 4 dai. The spectral signatures of infected spikes showed non-vegetative pattern in VIS-NIR range (Fig. 3c, f).

Spectral signature and spectral vegetation indices correlation with disease severity

To investigate the affected wavelengths by FHB, Pearson's coefficient between all spectral bands and disease severity was calculated (Fig. 4). For this approach, hyperspectral signatures were separated to identify important time periods in the pathogenesis in groups for 4–10 dai, 13–30 dai and 4–30 dai. High positive correlation ($r > 0.75$) has been shown in the spectral ranges 430–525 nm, 560–710 nm and 1115–2500 nm in all time period groups. Negative correlation ($r < -0.6$) has been shown in the spectral range 740–810 nm using the measurement time points 4–10 dai. This correlation decreased using 4–30 dai and 13–30 dai as data sets.

The fifteen proved vegetation indices which correlated with physiological parameters (Table 1), showed high correlation with disease severity (Fig. 5a). The indices NDVI, SIPI, PSNDa and PSNDb showed the highest absolute correlation with the disease severity ($r > 0.81$) in the VIS-NIR range 4 dai. Whereas in the SWIR, MSI reached a peak correlation with disease severity of $r = 0.9$. During the experimental period the absolute correlation between the calculated spectral indices and disease severity increased until 21 dai. In addition, mSR, PSSRa, PSSRb and CAI showed an increased absolute correlation until 30 dai.

Effect of FHB on spike weight and correlation with spectral vegetation indices

The loss in spike weight depended on the variety and the inoculated *Fusarium* species (Fig. 6). Reduction in

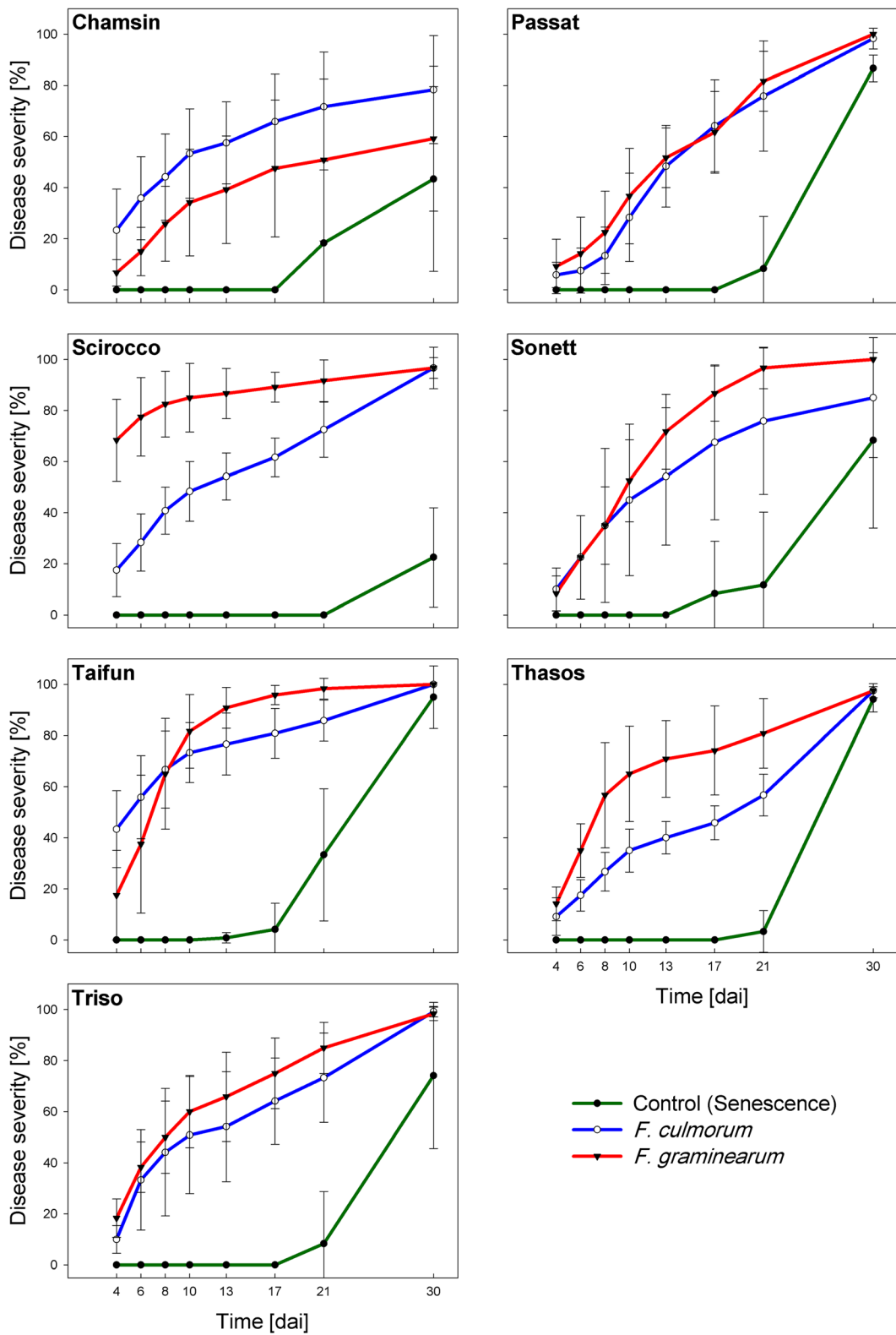


Fig. 2 Disease progress curve of wheat varieties inoculated with mock inoculation (water), *F. graminearum* and *F. culmorum* separately. (mean ± SD, n = 6)

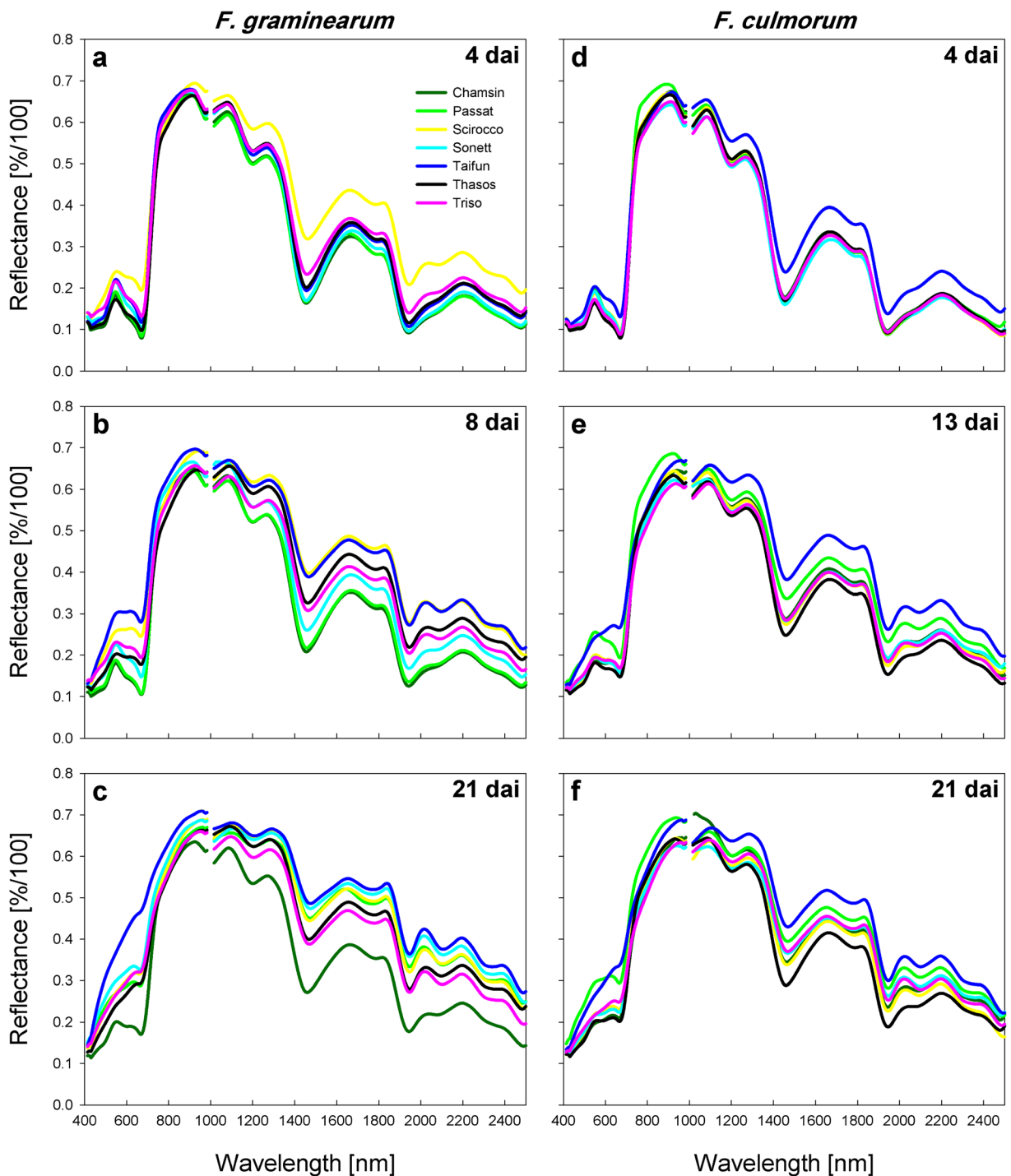


Fig. 3 Spectral signatures of *F. graminearum* infected spikes (a, b, c) 4, 8 and 21 dai respectively. *F. culmorum* infected spikes (d, e, f) 4, 13 and 21 dai respectively

spike weight caused by *F. graminearum* was higher than by *F. culmorum* in all varieties except Chamsin and Taifun. The spike weight reduction due to of

F. graminearum ranged between 30.86% in Taifun and 67.30% in Passat. The effect of *F. culmorum* ranged between 28.63% in Sonett and 51.84% in Chamsin.

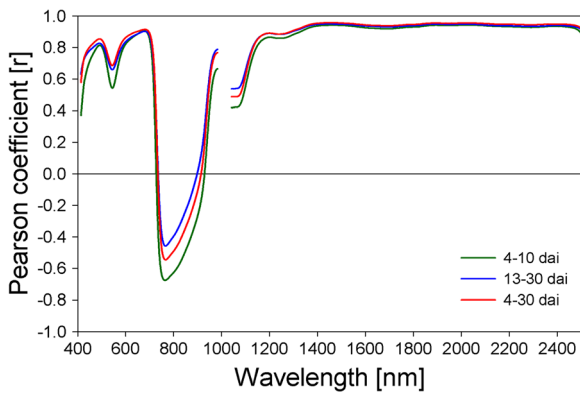
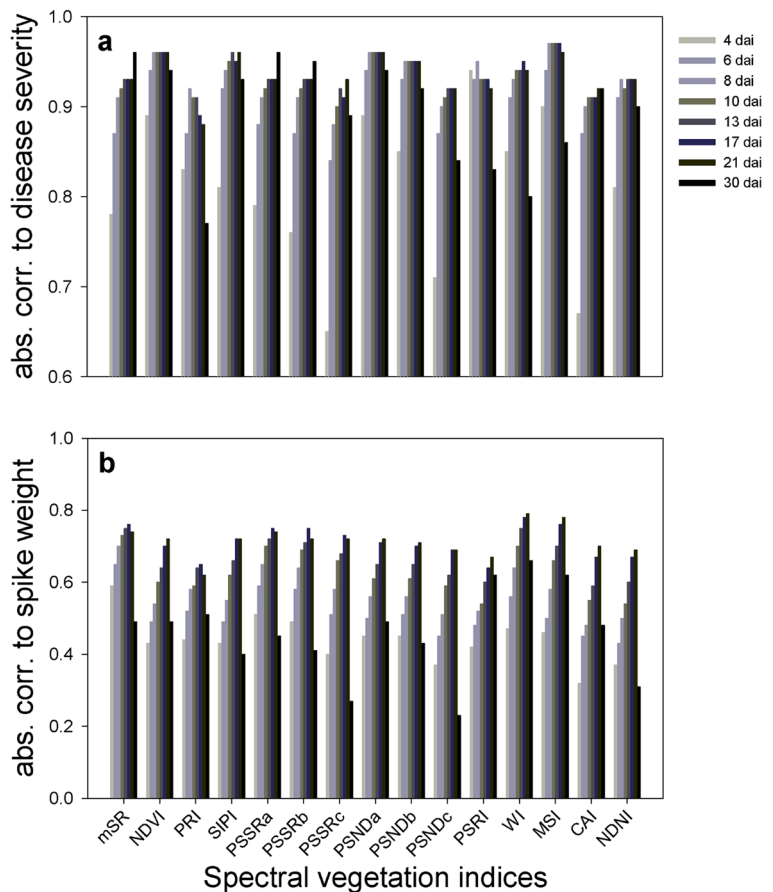


Fig. 4 Correlation between spectral signature and disease severity using the data 4–10 dai, 13–30 dai and 4–30 dai

SVIs showed gradual increased correlation overtime with spike weight at harvest until 13 dai or 21 dai depending on the specific index (Fig. 5b). For mSR the highest correlation was reached at 13 dai by $r = 0.75$. Afterwards, WI had the highest correlation with the spike weight reduction until 21 dai ($r = 0.79$).

Fig. 5 Correlation between spectral vegetation indices and disease severity (a), and correlation between spectral vegetation indices overtime and spike weight at harvest of wheat varieties (b)

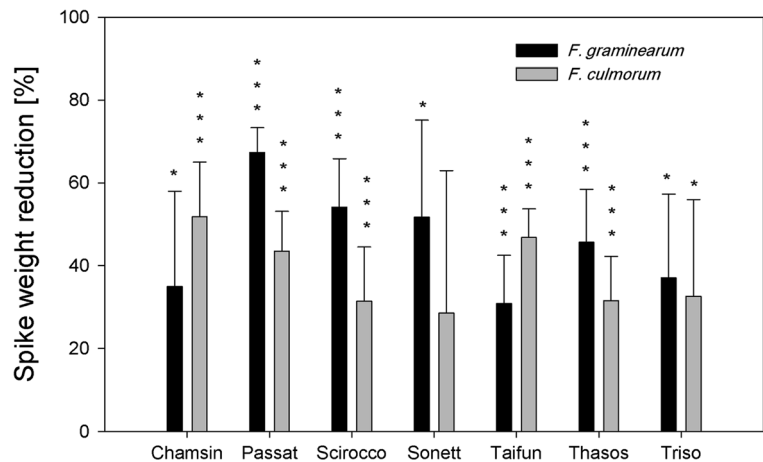


Two class and multiclass classification of control and FHB infected spikes

In the first step, SVM was used in two class classification to differentiate between healthy spikes and FHB infected spikes. Classification results based on SVIs calculated from VIS-NIR range were compared in their accuracies with the classification results based on spectral reflectance (Table 2). Both classification accuracies increased overtime with increasing disease severity until 4–8 dai and 13–17 dai. Thereafter, accuracies started to decrease when the natural senescence started in control spikes (Table 2). Except the first two measuring time points, the accuracy of spectral reflectance classification was higher than the accuracy of SVIs classification. In general, the accuracy was >0.76 in both cases and reached 0.99 at 13 and 17 dai for the classification based spectral reflectance.

Multiclass classification has been implemented to investigate the capability of SVM to discriminate healthy, *F. graminearum* and *F. culmorum* infected spikes. In case of

Fig. 6 Normalized reduction in spike weight of wheat varieties caused by *Fusarium* species. Data were analysed by standard analysis of variance (ANOVA, $n = 6$), marked by significance (*, $p \leq 0.05$) or high significance (***, $p \leq 0.001$)



SVIs classification, the accuracy increased gradually until 13 dai and reached 0.76, then slight decrease has been shown until the end of the experiment (Table 2). Accuracy of spectral reflectance classification fluctuated during the experimental period. The highest accuracy of 0.77 has been reached 13 dai. Except 6 dai, the accuracy was higher than >0.61 for all measured time points.

The confusion matrix at 13 dai shows that discrimination between control and *Fusarium* spp. infected spikes using SVM classification is possible with general accuracy of >0.76 (Table 3). Control spikes are better predicted with sensitivity of >0.97. Whereas, the prediction between *F. graminearum* and *F. culmorum* infected spikes is possible in advanced stages of infection with an average sensitivity of 0.65 (Table 3). Results of SVM multiclass classification based on hyperspectral data over the experimental period are indicated in Table S1.

Table 2 Accuracies of two class and multiclass SVM classification based on hyperspectral data overtime. Comparison between classification accuracies using twelve spectral vegetation indices (SVIs) and using the whole spectral reflectance 432 bands

Time	Two class classification		Multiclass classification	
	SVIs	Reflectance	SVIs	Reflectance
4	0.79	0.76	0.49	0.65
6	0.87	0.86	0.61	0.51
8	0.93	0.94	0.67	0.67
10	0.89	0.96	0.71	0.61
13	0.94	0.99	0.76	0.77
17	0.95	0.99	0.70	0.70
21	0.87	0.96	0.74	0.68
30	0.90	0.93	0.58	0.61

Variety ranking based on area under disease progress curve and non-metric multi-dimensional scaling

Spectral vegetation indices which are highly correlated to disease severity were selected due to their potential capability to differentiate between healthy and infected spikes. These SVIs were projected by NMDS onto a one-dimensional ordinal scale. This scale represents the disease severity sensed by the hyperspectral camera.

Figure 7 shows the variety ranking according to the area under disease progress curve (AUDPC) (Fig. 7a, c), and non-metric multidimensional scaling (NMDS) (Fig. 7b, d). The proved varieties showed different responses to the two investigated *Fusarium* species indicated in AUDPC (Fig. 7a, c). The varieties Scirocco and Taifun infected with *F. graminearum* showed high susceptibility with an AUDPC >2000 (Fig. 7a). In contrast, Chamsin showed moderate infestation with an AUDPC >1000. Most proved varieties revealed an AUDPC between 1300 and 1700 due to *F. culmorum* infection (Fig. 7c). High susceptibility to *F. culmorum* was only indicated by Taifun with an AUDPC >2000.

The results show that most proved varieties stayed in the same position in the ranking either using AUDPC or NMDS. Slight differences have been shown in variety order. The ranking of *F. graminearum* infected varieties (Fig. 7a, b) Thasos and Sonett differed two levels up and down using NMDS comparing to the AUDPC. *F. culmorum* infected variety Chamsin differed two levels up (Fig. 7c, d). Triso and Scirocco differed one-level down. Thasos and Passat exchanged their ranking using NMDS comparing to AUDPC.

Table 3 Confusion matrix of SVM multiclass classification 13 dai. Comparison between classification results using spectral vegetation indices (SVIs) (above), and using the whole spectral reflectance (below)

		Ground truth		
		Control	<i>F. culmorum</i>	<i>F. graminearum</i>
		SVI		
Prediction	Control	29	1	2
	<i>F. culmorum</i>	1	14	4
	<i>F. graminearum</i>	0	12	21
	Sensitivity	0.97	0.52	0.78
		Reflectance		
Prediction	Control	26	0	1
	<i>F. culmorum</i>	0	19	9
	<i>F. graminearum</i>	0	9	20
	Sensitivity	1	0.68	0.67

Discussion

The main effects of FHB on wheat spikes are chlorosis, collapse in spikelet tissue and disorder in the water

system of the spikelets and the spike. The extent and the dynamic of symptom development depend on the host plant resistance (Trail 2009; Ha et al. 2016; Al Masri et al. 2017). Former studies showed the feasibility

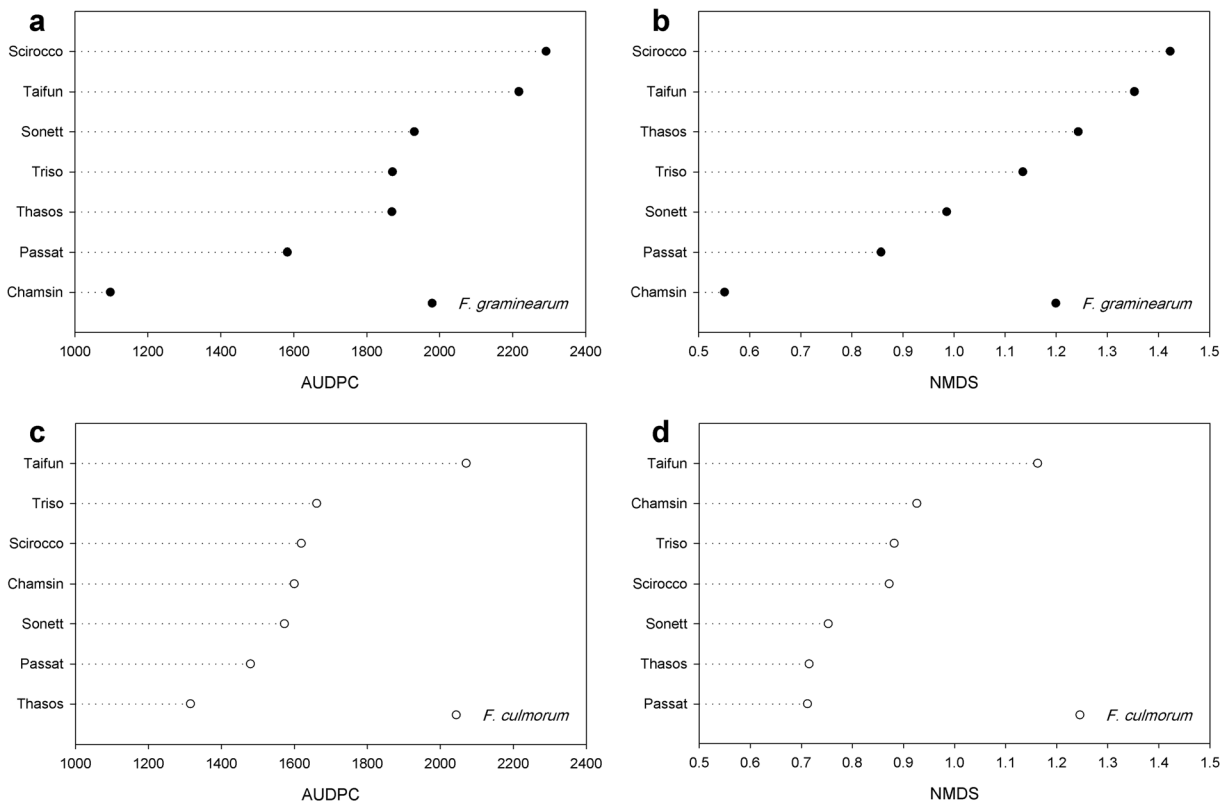


Fig. 7 Varieties ranking according to their susceptibility to FHB using Area under Disease Progress Curve (AUDPC) (a, c) and Non-metric multidimensional scaling (NMDS) (b, d)

of hyperspectral imaging to assess visible and non-visible symptoms caused by fungal diseases (Bauriegel et al. 2011; Delalieux et al. 2009; Mahlein et al. 2010). Characteristic spectral signatures in the VIS-NIR and SWIR are caused by alterations in pigment composition, tissue structure and plant water content (Mahlein 2016). In this study, the spectral reflectance was affected according to the susceptibility of wheat variety. The reflectance increased in VIS from 430 to 525 nm, 560–710 nm due to a rapid invasion of the pathogen which resulted in chlorophyll decomposition. The increase in reflectance intensity of susceptible varieties was higher compared to resistant varieties. Comparing *Fusarium* species, the reflectance in *F. graminearum* infected spikes was higher compared to *F. culmorum* infected spikes. This is presumably attributed to the high virulence of *F. graminearum* isolate used in this study comparing with *F. culmorum* isolate.

The correlation between disease severity and the individual spectral signature differs according to the symptoms caused by the pathogen (Mahlein et al. 2010). Plant senescence and chlorophyll decomposition result in an increase in reflectance intensity in the spectral ranges 400–530 nm and 550–740 nm (Merzlyak et al. 1999). This is consistent with the high correlation between the wavelengths from 430 to 525 nm and 560–710 nm and FHB disease severity confirmed in this study. Likewise, high correlation of SVIs derived from VIS-NIR range and disease severity has been confirmed.

Comparison between *Fusarium* spp. and *Cercospora beticola* shows that mycotoxins play a fundamental role in the pathogenicity resulting in collapse of tissue structure. *C. beticola* secretes cercosporin after penetrating the leaf through stomata (Daub and Ehrenshaft 2000). The main mycotoxins produced by *Fusarium* species is DON. High correlation was observed between DON concentration produced by isolates of *Fusarium* species and isolate virulence, where *Fusarium* species use DON as protein synthesis inhibitor to overcome the plant resistance (Rotter et al. 1996; Chetouhi et al. 2015; Kuhnem et al. 2015; Beukes et al. 2018).

In the NIR, Mahlein et al. (2010) proved a decrease in reflectance in the first stages of pathogenicity of *Cercospora beticola* on sugar beet leaves as a result of collapsed of tissue structure. In advanced stages, the reflectance increased again in this range. According to Leucker et al. (2016) the spectral reflectance in NIR was higher in susceptible varieties than resistant varieties and accompanied with higher sporulation density in

susceptible varieties of sugar beet. In case of FHB infection, the NIR reflectance of spikelet invaded with red *F. culmorum* mycelium was higher than areas showing only bleached symptoms (Bauriegel et al. 2011). Histological study of Ha et al. (2016) showed that dense growth of *F. graminearum* mycelium appeared more frequently and to a higher degree in the susceptible variety Milan than in the resistant variety Sumai-3. In the present study, the reflectance of spikes infected with both species was lower than reflectance of non-infected spikes in the NIR. However, correlation between varieties resistance and spectral reflectance in NIR could not be verified. The low correlation in NIR may be due to the three dimensional structure of wheat spike. Further investigations on spikelet scale are still needed to correlate the reflectance in NIR with sporulation density, mycelium growth and variety resistance.

One of the main effects of FHB progress is early senescence (Trail 2009). The SWIR component of the electromagnetic spectrum was highly correlated to the water content, and might therefore serve as a proxy for early senescence and FHB progress. Following, high correlation of DS with the spectral range in the SWIR was indicated. The reflectance in SWIR differed depending on susceptibility of each variety. A high susceptibility to FHB is related to an early senescence and fast draining in spike water and as a result, higher reflectance in SWIR. This is in accordance with results presented by Iori et al. (2015). They proved the increase in reflectance in the SWIR over time in wheat varieties infected with *Stagonospora nodorum*. Comparing two apple varieties with different susceptibility to apple scab (*Venturia inaequalis*) showed higher reflectance in SWIR in susceptible variety than in resistant one, respectively (Delalieux et al. 2009).

Several studies showed significant effect of *Fusarium* infection on the kernel protein content which is correlated to the kernel nitrogen concentration. The crude protein content increased due to *Fusarium* infection whereas the total glutenin and high-molecular-weight glutenin content decreased significantly in the wheat kernels resulted from *Fusarium* infected spikes (Wang et al. 2005; Siuda et al. 2010; Kreuzberger et al. 2015). In this study, and for the first time, three indices derived from SWIR range related to nitrogen (NDNI), cellulose (CAI) and water stress (MSI) showed high correlation with FHB severity.

However, effective approaches for analysing the obtained hyperspectral data with its high complexity are

required. Machine learning approaches showed high capacities in hyperspectral data analysis and the potential to accelerate screening processes in plant resistance breeding (Rumpf et al. 2010; Behmann et al. 2015; Singh et al. 2016). In the present study, SVM classification was applied in multiple settings regarding time classes and features. The decrease in accuracy in later stages of FHB pathogenesis is due to the senescence in control spikes. The classification accuracy was lower using the SVIs than using the whole spectral reflectance which considered the water stresses detected in the SWIR caused by FHB. Interestingly, it was possible to differentiate between the infections of two *Fusarium* species by multiclass classification. This result could be due to the differences in the isolates virulence more than differences in symptoms caused by the both species.

The lack in FHB resistant varieties requires more efforts to investigate new resistance sources through wild and domesticated wheat germplasm diversity (Steiner et al. 2017). Due to the difficulties in Type I resistance assessment, most QTLs have been identified to be involved in Type II resistance (Buerstmayr et al. 2009; Steiner et al. 2017). Mesterházy et al. (2007) emphasized the necessity of including Type I resistance in breeding programs. The traditional rating of plant disease severity depends on AUDPC which is used to combine multiple observations of disease severity into a single value (Simko and Piepho 2012). It has been shown that the AUDPC can be reproduced with high accuracy by the combination of multiple SVIs transformed by NMDS. The differences in varieties ranking using the traditional AUDPC and NMDS could be attributed to two factors which were taken into account in NMDS approach. The first, the data of control plants has been subtracted to omit the natural senescence. The second, the data of the first and the last measuring dates has been neglected to exclude the extreme values.

During the last decades, the FHB epidemic frequency increased in the main wheat production regions in the world. This could be attributed to the changes in the agricultural practices like reduced tillage, and the intensification of maize which is one of the main hosts of FHB in crop rotation (McMullen et al. 2012). Many studies monitored the geographic specificity in *F. graminearum* and *F. culmorum* chemotypes in wheat producing countries (Ward et al. 2008; Talas et al. 2011; Alkadri et al. 2014; van der Lee et al. 2015; Pasquali et al. 2016). They identified the changes in *Fusarium* dominant chemotypes during a short time. This

emphasises the need for continuous development of varieties with resistance to a wide range not only of *Fusarium* species but also of *Fusarium* chemotypes. Here, hyperspectral imaging and sophisticated machine learning approaches, as investigated in this study can improve the FHB resistance breeding process by an accelerated wheat resistance identification and characterization. New handheld hyperspectral cameras increase the flexibility and usability also by non-experts in the field (Behmann et al. 2018). These approaches assist e.g. the breeder for an improved determination of relevant wheat varieties.

Conclusions

Hyperspectral imaging is a state-of-the-art technology and method for plant sciences and may be applied in plant resistance breeding. In addition to the assessment of the dynamics of FHB symptoms, it was feasible to differentiate not only between *Fusarium* infected spikes and healthy ones, but also between spikes infected with different *Fusarium* species by a SVM classification. As an important outcome, an automated method to reproduce AUDPC depending on seven SVIs derived from the electromagnetic spectrum in VIS, NIR and SWIR was established. This will improve the automation in disease rating and will provide more objective information for the decision making process in resistance breeding.

Acknowledgements This study was funded by the German Federal Ministry of Education and Research (BMBF) within the scope of the competitive grants program “Networks of excellence in agricultural and nutrition research - CROP.SENSE.net” (Funding code: 0315529), Junior Research Group “Hyperspectral phenotyping of resistance reactions of barley” and due to financial support of the Catholic Academic Exchange Service (KAAD).

References

- Al Masri, A., Hau, B., Dehne, H.-W., Mahlein, A.-K., & Oerke, E.-C. (2017). Impact of primary infection site of *Fusarium* species on head blight development in wheat ears evaluated by IR-thermography. *European Journal of Plant Pathology*, *147*, 855–868.
- Alkadri, D., Rubert, J., Prodi, A., Pisi, A., Manes, J., & Soler, C. (2014). Natural co-occurrence of mycotoxins in wheat grains from Italy and Syria. *Food Chemistry*, *157*, 111–118.
- Aoki, T., O'Donnell, K., & Geiser, D. M. (2014). Systematics of key phytopathogenic *Fusarium* species: Current status and

- future challenges. *Journal of General Plant Pathology*, *80*, 189–201.
- Bauriegel, E., Giebel, A., Geyer, M., Schmidt, U., & Herppich, W. B. (2011). Early detection of *Fusarium* infection in wheat using hyper-spectral imaging. *Computer and Electronics in Agriculture*, *75*, 304–312.
- Behmann, J., Mahlein, A.-K., Rumpf, T., Römer, C., & Plümer, L. (2015). A review of advanced machine learning methods for the detection of biotic stress in precision crop protection. *Precision Agriculture*, *16*, 239–260.
- Behmann, J., Acebron, K., Emin, D., Bennertz, S., Matsubara, S., Thomas, S., Bohnenkamp, D., Kuska, M. T., Jussila, J., Salo, H., Mahlein, A. K., & Rascher, U. (2018). Specim IQ: Evaluation of a new, miniaturized handheld hyperspectral camera and its application for plant phenotyping and disease detection. *Sensors*, *18*, 441.
- Beukes, I., Rose, L. J., van Coller, G. J., & Viljoen, A. (2018). Disease development and mycotoxin production by the *Fusarium graminearum* species complex associated with south African maize and wheat. *European Journal of Plant Pathology*, *150*, 893–910.
- Birzele, B., Meier, A., Hindorf, H., Krämer, J., & Dehne, H.-W. (2002). Epidemiology of *Fusarium* infection and Deoxynivalenol content in winter wheat in the Rhineland, Germany. *European Journal of Plant Pathology*, *108*, 667–673.
- Blackburn, G. A. (1998a). Quantifying chlorophylls and carotenoids at leaf and canopy scale: An evaluation of some hyperspectral approaches. *Remote Sensing of Environment*, *66*, 273–285.
- Blackburn, G. A. (1998b). Spectral indices for estimating photosynthetic pigment concentrations: A test using senescent tree leaves. *International Journal of Remote Sensing*, *19*, 657–675.
- Borg, I., & Groenen, P. (2005). *Modern multidimensional scaling: Theory and applications* (2nd ed.). New York: Springer-Verlag.
- Brown, N. A., Urban, M., van deMeene, A. M. L., & Hammond-Kosack, K. E. (2010). The infection biology of *Fusarium graminearum*: Defining the pathways of spikelet to spikelet colonisation in wheat ears. *Fungal Biology*, *114*, 555–571.
- Buerstmayr, H., Ban, T., & Anderson, J. A. (2009). QTL mapping and marker-assisted selection for *Fusarium* head blight resistance in wheat; a review. *Plant Breeding*, *128*, 1–26.
- Bushnell, W. R., Hazen, B. E., & Pritsch, C. (2003). Histology and physiology of *Fusarium* head blight. In K. J. Leonard & W. R. Bushnell (Eds.), *Fusarium head blight of wheat and barley* (pp. 44–83). St. Paul, Minnesota: APS Press.
- Chetouhi, C., Bonhomme, L., Lecomte, P., Cambon, F., Merlino, M., Biron, D. G., & Langin, T. (2015). A proteomics survey on wheat susceptibility to *Fusarium* head blight during grain development. *European Journal of Plant Pathology*, *141*, 407–418.
- Cortes, C., & Vapnik, N. V. (1995). Support-vector networks. *Machine Learning*, *20*, 273–297.
- Daub, M. E., & Ehrenshaft, M. (2000). The photoactivated *Cercospora* toxin cercosporin: Contributions to plant disease and fundamental biology. *Annual Review of Phytopathology*, *38*, 461–490.
- Daughtry, C. S. T. (2001). Discriminating crop residues from soil by shortwave infrared reflectance. *Agronomy Journal*, *93*, 125–131.
- Delalieux, S., Somers, B., Verstraeten, W. W., van Aardt, J. A. N., Keulemans, W., & Coppin, P. (2009). Hyperspectral indices to diagnose leaf biotic stress of apple plants, considering leaf phenology. *International Journal of Remote Sensing*, *30*, 1887–1912.
- van der Lee, T., Zhang, H., van Diepeningen, A., & Waalwijk, C. (2015). Biogeography of *Fusarium graminearum* species complex and chemotypes: A review. *Food Additives & Contaminants: Part A*, *32*, 453–460.
- Descriptive List of Varieties, Bundessortenamt, Germany. (2017). Getreide, Mais, Öl- und Faserpflanzen, Leguminosen, Rüben, Zwischenfrüchte. In *Bundessortenamt. Deutschland: Hannover* https://www.bundessortenamt.de/internet30/index.php?id=41&tx_ttnews%5Btt_news%5D=308&cHash=bb2220e6c08a91dfd6a99e8fd6f575a3.
- Dweba, C. C., Figlan, S., Shimelis, H. A., Motaung, T. E., Sydenham, S., Mwadzingeni, L., & Tsilo, T. J. (2017). *Fusarium* head blight of wheat: Pathogenesis and control strategies. *Crop Protection*, *91*, 114–122.
- Fahlgren, N., Feldman, M., Gehan, M., Wilson, M. S., Shyu, C., Bryant, D. W., Hill, S. T., McEntee, C. J., Warnasooriya, S. N., Kumar, I., Ficor, T., Turnipseed, S., Gilbert, K. B., Brutnell, T. P., Carrington, J. C., Mockler, T. C., & Baxter, I. (2015). A versatile phenotyping system and analytics platform reveals diverse temporal responses to water availability in *Setaria*. *Molecular Plant*, *8*, 1–16.
- Ferrigo, D., Alessandro Raiola, A., & Roberto, R. (2016). *Fusarium* toxins in cereals: Occurrence, legislation, factors promoting the appearance and their management. *Molecules*, *21*, 627.
- Furbank, R. T., & Tester, M. (2011). Phenomics - technologies to relieve the phenotyping bottleneck. *Trends in Plant Science*, *16*, 635–644.
- Gamon, J. A., Peñuelas, J., & Field, C. B. (1992). A narrow-waveband spectral index that tracks diurnal changes in photosynthetic efficiency. *Remote Sensing of Environment*, *41*, 35–44.
- Gilbert, J., & Haber, S. (2013). Overview of some recent research developments in *Fusarium* head blight of wheat. *Canadian Journal of Plant Pathology*, *35*, 149–174.
- Ha, X., Koopmann, B., & von Tiedemann, A. (2016). Wheat blast and *Fusarium* head blight display contrasting interaction patterns on ears of wheat genotypes differing in resistance. *Phytopathology*, *106*, 270–281.
- Hunt, E., & Rock, B. (1989). Detection of changes in leaf water-content using near-infrared and middle-infrared reflectances. *Remote Sensing of Environment*, *30*, 43–54.
- Iori, A., Scala, V., Cesar, D., Pinzari, F., D'Egidio, M. G., Fanelli, C., Fabbri, A. A., Reverberi, M., & Serranti, S. (2015). Hyperspectral and molecular analysis of *Stagonospora nodorum* blotch disease in durum wheat. *European Journal of Plant Pathology*, *141*, 689–702.
- Johnson, D. D., Flakerud, G. K., Taylor, R. D., & Satyanarayana, V. (2003). Quantifying economic impacts of *Fusarium* head blight in wheat. In K. J. Leonard & W. R. Bushnell (Eds.), *Fusarium head blight of wheat and barley* (pp. 461–484). St. Paul, Minnesota: APS Press.
- Kreuzberger, M., Limsuwan, S., Eggert, K., Karlovsky, P., & Pawelzik, E. (2015). Impact of *Fusarium* spp. infection of bread wheat (*Triticum aestivum* L.) on composition and quality of flour in association with EU maximum level for

- deoxynivalenol. *Journal of Applied Botany and Food Quality*, 88, 177–185.
- Kruskal, J. B. (1964). Multidimensional scaling by optimizing goodness of fit to a nonmetric hypothesis. *Psychometrika*, 29, 1–27.
- Kuhnem, P. R., Del Ponte, E. M., Dong, Y., & Bergstrom, G. C. (2015). *Fusarium graminearum* isolates from wheat and maize in New York show similar range of aggressiveness and Toxigenicity in cross-species pathogenicity tests. *Phytopathology*, 105, 441–448.
- Kuska, M. T., & Mahlein, A.-K. (2018). Aiming at decision making in plant disease protection and phenotyping by the use of optical sensors. *European Journal of Plant Pathology*. <https://doi.org/10.1007/s10658-018-1464-1>.
- Kuska, M. T., Brugger, A., Thomas, S., Wahabzada, M., Kersting, K., Oerke, E. C., Steiner, U., & Mahlein, A. K. (2017). Spectral patterns reveal early resistance reactions of barley against *Blumeria graminis* f. Sp. *hordei*. *Phytopathology*, 107, 1388–1398.
- Lancashire, P. D., Bleiholder, H., Van den Boom, T., Langeluddecke, P., Stauss, R., Weber, E., & Witzemberger, A. (1991). A uniform decimal code for growth stages of crops and weeds. *Annals of Applied Biology*, 119, 561–601.
- Leucker, M., Mahlein, A.-K., Steiner, U., & Oerke, E.-C. (2016). Improvement of lesion phenotyping in *Cercospora beticola*-sugar beet interaction by hyperspectral imaging. *Phytopathology*, 106, 177–184.
- Mahlein, A.-K. (2016). Present and future trends in plant disease detection. *Plant Disease*, 100, 241–251.
- Mahlein, A.-K., Steiner, U., Dehne, H.-W., & Oerke, E.-C. (2010). Spectral signatures of sugar beet leaves for the detection and differentiation of diseases. *Precision Agriculture*, 11, 413–431.
- Mahlein, A.-K., Steiner, U., Hillnhütter, C., Dehne, H.-W., & Oerke, E.-C. (2012). Hyperspectral imaging for small-scale analysis of symptoms caused by different sugar beet diseases. *Plant Methods*, 8, 3.
- McCormick, S. (2003). The role of DON in pathogenicity. In K. J. Leonard & W. R. Bushnell (Eds.), *Fusarium head blight of wheat and barley* (pp. 165–183). St. Paul, Minnesota: APS Press.
- McMullen, M., Bergstrom, G., De Wolf, E., Dill-Macky, R., Hershman, D., Shaner, G., & Van Sanford, D. (2012). A unified effort to fight an enemy of wheat and barley: *Fusarium* head blight. *Plant Disease*, 96, 1712–1728.
- Merzlyak, M. N., Gitelson, A. A., Chivkunova, O. B., & Rakitin, V. Y. (1999). Non-destructive optical detection of pigment changes during leaf senescence and fruit ripening. *Physiologica Plantarum*, 106, 135–141.
- Mesterházy, Á., Buerstmayr, H., Tóth, B., Lehoczki-Krsjak, Sz., Szabó-Hevér, Á., & Lemmens, M. (2007). An improved strategy for breeding FHB resistant wheat must include type I resistance. In Proceedings of the 5th Canadian workshop on *Fusarium* head blight, 27–30 November 2007, Delta Winnipeg (Canada), 51–66.
- Mesterházy, Á., Lehoczki-Krsjak, S., Varga, M., Szabó-Hevér, Á., Tóth, B., & Lemmens, M. (2015). Breeding for FHB resistance via *Fusarium* damaged kernels and Deoxynivalenol accumulation as well as inoculation methods in winter wheat. *Agricultural Sciences*, 6, 970–1002.
- Moradi, G. M. (2008). Microbiological and molecular assessment of interactions among the major *Fusarium* head blight pathogens on wheat ear. In Bonn, Germany: University of Bonn. PhD thesis.
- Nagler, P. L., Inoue, Y., Glenn, E. P., Russ, A. L., & Daughtry, C. S. T. (2003). Cellulose absorption index (CAI) to quantify mixed soil–plant litter scenes. *Remote Sensing of Environment*, 87, 310–325.
- O'Donnell, K., Ward, T. J., Geiser, D. M., Kistler, H. C., & Aoki, T. (2004). Genealogical concordance between the mating type locus and seven other nuclear genes supports formal recognition of nine phylogenetically distinct species within the *Fusarium graminearum* clade. *Fungal Genetics and Biology*, 41, 600–623.
- Osborne, L. M., & Stein, J. M. (2007). Epidemiology of *Fusarium* head blight on small-grain cereals. *International Journal of Food Microbiology*, 119, 103–108.
- Parry, D. W., Jenkinson, P., & McLeod, L. (1995). *Fusarium* ear blight (scab) in small grain cereals—a review. *Plant Pathology*, 44, 207–238.
- Pasquali, M., Beyer, M., Logrieco, A., Audenaert, K., Balmas, V., Basler, R., Boutigny, A.-L., Chrpová, J., Czembor, E., Gagkaeva, T., González-Jaén, M. T., Hofgaard, I. S., Köycü, N. D., Hoffmann, L., Levic, J., Marin, P., Miedaner, T., Migheli, Q., Moretti, A., Müller, M. E. H., Munaut, F., Parikka, P., Pallez-Barthel, M., Piec, J., Scauflaire, J., Scherm, B., Stankovic, S., Thrane, U., Uhlig, S., Vanheule, A., Yli-Mattila, T., & Vogelgsang, S. (2016). A European database of *Fusarium graminearum* and *F. culmorum* trichothecene genotypes. *Frontiers in Microbiology*, 7, 406.
- Peñuelas, J., Baret, F., & Filella, I. (1995). Semiempirical indices to assess carotenoids/chlorophyll a ratio from leaf spectral reflectance. *Photosynthetica*, 31, 221–230.
- Peñuelas, J., Pinol, R. O., Ogaya, R., & Filella, I. (1997). Estimation of plant water concentration by the reflectance water index WI (R900/R970). *International Journal of Remote Sensing*, 18, 2869–2875.
- Pestka, J. J. (2010). Deoxynivalenol: Mechanisms of action, human exposure, and toxicological relevance. *Archives of Toxicology*, 84, 663–679.
- Ribichich, K. F., Lopez, S. E., & Vegetti, A. C. (2000). Histopathological spikelet changes produced by *Fusarium graminearum* in susceptible and resistant wheat cultivars. *Plant Disease*, 84, 794–802.
- Rotter, B. A., Prelusky, D. B., & Pestka, J. J. (1996). Toxicology of deoxynivalenol (vomitoxin). *Journal of Toxicology and Environmental Health*, 48, 1–34.
- Rouse, J. W., Haas, R. H., Schell, J. A., & Deering, D. W. (1974). Monitoring vegetation systems in the Great Plains with ERTS. In Proceedings 3th Earth Resources Technology Satellite-1 Symposium, Goddard Space Flight Center, 10–14 December 1973, NASA, Washington, D.C. (USA), 309–317.
- Rumpf, T., Mahlein, A.-K., Steiner, U., Oerke, E.-C., Dehne, H.-W., & Plümer, L. (2010). Early detection and classification of plant diseases with support vector machines based on hyperspectral reflectance. *Computers and Electronics in Agriculture*, 74, 91–99.
- Salgado, J. D., Madden, L. V., & Paul, P. A. (2015). Quantifying the effects of *Fusarium* head blight on grain yield and test

- weight in soft red winter wheat. *Phytopathology*, *105*, 295–306.
- Schroeder, H. W., & Christensen, J. J. (1963). Factors affecting resistance of wheat to scab caused by *Gibberella zeae*. *Phytopathology*, *53*, 831–838.
- Serrano, L., Peñuelas, J., & Ustin, S. L. (2002). Remote sensing of nitrogen and lignin in Mediterranean vegetation from AVIRIS data: Decomposing biochemical from structural signals. *Remote Sensing of Environment*, *81*, 355–364.
- Simko, I., & Piepho, H.-P. (2012). The area under the disease progress stairs: Calculation, advantage, and application. *Phytopathology*, *102*, 381–389.
- Sims, D. A., & Gamon, J. A. (2002). Relationship between leaf pigment content and spectral reflectance across a wide range of species, leaf structures and developmental stages. *Remote Sensing of Environment*, *81*, 337–354.
- Singh, A., Ganapathysubramanian, B., Singh, A. K., & Sarkar, S. (2016). Machine learning for high-throughput stress phenotyping in plants. *Trends in Plant Science*, *21*, 110–124.
- Siuda, R., Grabowski, A., Lenc, L., Ralcewicz, M., & Spychaj-Fabisiak, E. (2010). Influence of the degree of fusariosis on technological traits of wheat grain. *International Journal of Food Science and Technology*, *45*, 2596–2604.
- Stack, R. W., & McMullen, M. P. (1995). A visual scale to estimate severity of *Fusarium* head blight in wheat. North Dakota State University Extension Service, PP-1095.
- Steiner, B., Buerstmayr, M., Michel, S., Schweiger, W., Lemmens, M., & Buerstmayr, H. (2017). Breeding strategies and advances in line selection for *Fusarium* head blight resistance in wheat. *Tropical Plant Pathology*, *42*, 165–174.
- Talas, F., Parzies, H. K., & Miedaner, T. (2011). Diversity in genetic structure and chemotype composition of *Fusarium graminearum* sensu stricto populations causing wheat head blight in individual fields in Germany. *European Journal of Plant Pathology*, *131*, 39–48.
- Thomas, S., Wahabzada, M., Kuska, M.-T., Rascher, U., & Mahlein, A.-K. (2016). Observation of plant–pathogen interaction by simultaneous hyperspectral imaging reflection and transmission measurements. *Functional Plant Biology*, *44*, 23–34.
- Thomas, S., Kuska, M.-T., Bohnenkamp, D., Brugger, A., Alisaac, E., Wahabzada, M., Behmann, J., & Mahlein, A.-K. (2018). Benefits of hyperspectral imaging for plant disease detection and plant protection: A technical perspective. *Journal of Plant Diseases and Protection*, *125*, 5–20.
- Trail, F. (2009). For blighted waves of grain: *Fusarium graminearum* in the postgenomics era. *Plant Physiology*, *149*, 103–110.
- Wang, J., Wieser, H., Pawelzik, E., Weinert, J., Keutgen, A. J., & Wolf, G. A. (2005). Impact of the fungal protease produced by *Fusarium culmorum* on the protein quality and breadmaking properties of winter wheat. *European Food Research and Technology*, *220*, 225–259.
- Ward, T. J., Clear, R. M., Rooney, A. P., O'Donnell, K., Gaba, D., Patrick, S., Starkey, D. E., Gilbert, J., Geiser, D. M., & Nowicki, T. W. (2008). An adaptive evolutionary shift in *Fusarium* head blight pathogen populations is driving the rapid spread of more toxigenic *Fusarium graminearum* in North America. *Fungal Genetics and Biology*, *45*, 473–484.
- Xue, J., & Su, B. (2017). Significant remote sensing vegetation indices: A review of developments and applications. *Journal of Sensors*, article ID, 1353691 17 Pages.